Available online at www.sciencedirect.com
ScienceDirect
Journal of Catalysis 245 (2007) 358–368
JOURNAL OF CATALYSIS
www.elsevier.com/locate/jcat

Direct NO and N_2O decomposition and NO-assisted N_2O decomposition over Cu-zeolites: Elucidating the influence of the Cu–Cu distance on oxygen migration

Pieter J. Smeets [a], Marijke H. Groothaert [a,1], Robert M. van Teeffelen [b], Hugo Leeman [a], Emiel J.M. Hensen [b], Robert A. Schoonheydt [a,*]

[a] *Center for Surface Chemistry and Catalysis, K.U. Leuven, Kasteelpark Arenberg 23, B-3001 Leuven, Belgium*
[b] *Schuit Institute of Catalysis, Eindhoven University of Technology, P.O. Box 513, 5600 MB Eindhoven, The Netherlands*

Received 28 June 2006; revised 13 October 2006; accepted 17 October 2006

Available online 28 November 2006

Abstract

Several zeolites of varying topology and with different Cu/Al ratios were investigated in the catalytic decomposition of NO, N_2O and the NO-assisted N_2O decomposition. The highest activity in the direct NO and N_2O decomposition was found for bis(μ-oxo)dicopper cores in Cu-ZSM-5 followed by the EPR silent Cu in MOR, FER and BEA, while almost no activity was observed over the isolated, EPR detectable Cu sites. This sequence of decreasing activity follows the increasing average distance between Cu sites. An average volume of 35 Å^3 per Cu atom (average Cu–Cu distance 4.1 Å) appears to be a threshold value separating high and low activity. The high activity for catalysts with small Cu–Cu distances is explained by facile oxygen migration over the Cu sites, enabling recombination into gaseous O_2. When the distance between the Cu centers is increased, oxygen migration is hampered. Adding NO results in the scavenging of the deposited O atoms, thereby transporting them into the gas phase. Hence an alternative oxygen migration pathway is created that has the greatest impact on activity of the isolated EPR-detectable Cu sites and a negative effect on the bis(μ-oxo)dicopper cores in Cu-ZSM-5.

Keywords: N_2O decomposition; NO decomposition; NO-assisted; N_2O decomposition; Copper zeolites; Bis(μ-oxo)dicopper core; EPR silent copper

1. Introduction

Since the discovery by Iwamoto [1] that overexchanged Cu-ZSM-5 zeolites have high activity in the decomposition of NO into N_2 and O_2, Cu-zeolites have been studied in detail. Cu-ZSM-5 is active in a wide range of reactions of nitrogen oxides, including (photo) catalytic decomposition of NO and N_2O, catalytic reduction of NO with CO and hydrocarbons, and selective catalytic reduction of NO with NH_3 [2]. So far, commercial deNO_x applications of Cu-ZSM-5 include (i) high-temperature reduction of stationary NO_x emissions using NH_3 and (ii) lean NO_x reduction for diesel vehicles, as communicated by Jobson [3]. Although over the past 20 years a consensus has developed as to the catalytic performance of these materials, identification of the active sites remains a matter of debate [4,5]. Recently, we studied the catalytic NO decomposition using operando UV–vis spectroscopy, which led to the insight that the bis(μ-oxo)dicopper core plays a key role in catalysis [6–8]. During NO decomposition, oxygen-bridged Cu dimers are formed, allowing easy desorption of molecular oxygen, which is the rate-limiting step. Moreover, we have shown that the bis(μ-oxo)dicopper core can selectively oxidize methane into methanol [9,10].

Besides Cu-ZSM-5, also other transition metal ion (TMI)-exchanged zeolites (Cu, Fe, and Co) have been reported to be active in the direct decomposition of NO and N_2O [11–22] and in the selective catalytic reduction (SCR) of NO_x and N_2O using light hydrocarbons [23–33], NH_3 [30,32,34–39], or ureum [40–42]. Recently, NO-assisted N_2O decomposition us-

* Corresponding author. Fax: +32 16 321998.
E-mail address: robert.schoonheydt@biw.kuleuven.be (R.A. Schoonheydt).
[1] Current address: DSM, P.O. Box 18, 6160 MD Geleen, The Netherlands.

0021-9517/$ – see front matter
doi:10.1016/j.jcat.2006.10.017

ing Fe-ZSM-5 zeolites yielded very promising results with a possible use in tail gas cleaning of nitric acid plants [43–53]. Small amounts of NO strongly increase the decomposition of N_2O into harmless oxygen and nitrogen. Consensus about the reaction mechanism of this NO-assisted N_2O decomposition has not been reached; several possible reaction pathways have been suggested by Moulijn and co-workers [43,51] and Sang et al. [49]. NO can be considered a storage or transport medium for O atoms deposited by N_2O on the surface, facilitating the recombination of two O atoms. This has a significant effect on overall N_2O decomposition activity, because reduced Fe species can easily abstract O atoms from N_2O [25,54–56] but the release of O_2 is often hampered [20].

The activities of the Cu-based catalysts for the direct decomposition of NO or N_2O presented in the literature are difficult to compare because often different reaction conditions are used and the reactions investigated are not the same for all of the Cu-zeolites. Consequently, in this work, 13 Cu-exchanged zeolites were compared under equal reaction conditions in a parallel reactor setup. Along with direct NO and N_2O decomposition, NO-assisted N_2O decomposition was also investigated. FTIR and UV–vis spectra were collected during the NO-assisted N_2O decomposition to elucidate the effect of NO. Two different Cu loadings were investigated for each topology (MOR, FER, BEA). For Cu-ZSM-5, a series of catalysts with increasing Cu/Al ratio was tested to link activity data to the presence of the bis(μ-oxo)dicopper core.

2. Experimental

2.1. Preparation of Cu^{2+} exchanged zeolites

The characteristics of all prepared Cu^{2+} zeolite materials are summarized in Table 1. The zeolites were first exchanged with $NaNO_3$ followed by Cu^{2+} exchange, according to a previously published procedure [9,10]. The as-prepared samples are denoted as CX-Y-Z, where X stands for the first letter of the zeolite (Z = ZSM-5, M = MOR, B = BEA, and F = FER), Y is the Si/Al ratio, and Z the Cu/Al ratio. The Cu and Al contents were determined by inductively coupled plasma (ICP) after dissolution of the samples in HF.

Table 1
Chemical and structural details of the catalysts

Sample	Source	Topology	Si/Al	Cu/Al	Cu (wt%)
CZ-12-0.56	ALSI-PENTA	MFI	12	0.56	4.3
CZ-12-0.42	ALSI-PENTA	MFI	12	0.42	3.1
CZ-12-0.29	ALSI-PENTA	MFI	12	0.29	2.3
CZ-12-0.22	ALSI-PENTA	MFI	12	0.22	1.8
CZ-12-0.10	ALSI-PENTA	MFI	12	0.10	0.9
CM-5.3-0.39	Norton	MOR	5.3	0.39	4.8
CM-5.3-0.22	Norton	MOR	5.3	0.22	2.7
CM-8.8-0.50	TRICAT	MOR	8.8	0.50	5.4
CM-8.8-0.20	TRICAT	MOR	8.8	0.20	2.1
CF-6.2-0.42	Toyo Soda	FER	6.2	0.42	6.1
CF-6.2-0.21	Toyo Soda	FER	6.2	0.21	3.1
CB-9.8-0.38	ZEOCAT^{TM}	BEA	9.8	0.38	2.8
CB-9.8-0.17	ZEOCAT^{TM}	BEA	9.8	0.17	1.3

2.2. Catalyst characterization

2.2.1. EPR

The samples were pelletized (0.25–0.5 mm) and brought into quartz flow cells with a suprasil window for diffuse reflectance spectroscopy (DRS) and a quartz sidearm for electron paramagnetic resonance (EPR) measurements. Before these measurements, the samples were treated in flowing O_2 (50 ml/min) from room temperature (RT) up to 450 °C at a ramp rate of 1 °C/min. The samples were kept overnight in O_2 flow. After the samples were cooled in a closed O_2 atmosphere and flushed with He for 60 s at room temperature, X-band EPR spectra were recorded at 120 K with a Bruker ESP 300E instrument in a rectangular TE104 cavity. Spin concentrations were calculated by double integration of the first derivative spectra. KCl-diluted $Cu(acac)_2$ standards (acac = acetylacetonate) of known spin concentration were used to obtain a calibration curve. The absolute margin of error on the calculated spin concentrations is estimated to be <20% [57].

2.2.2. Fourier transform infrared spectroscopy (FTIR)

An inox infrared cell with CaF_2 windows was used for the FTIR measurements at high temperature (300 and 450 °C). This cell can be heated to temperatures as high as 580 °C, while cooling water removes excess heat from the CaF_2 windows and O-ring seals [58]. The zeolite samples were introduced as self-supporting wafers with an average weight of 10 mg/cm^2. The wafers were treated in flowing He (50 ml/min) while being heated from RT to 450 °C at a ramp rate of 1 °C/min, where they were kept overnight. After the wafers were cooled in flowing He to the reaction temperature, the experiments were started.

Infrared measurements were performed on a Nicolet 730 FTIR spectrometer equipped with a DTGS detector. Typically, one spectrum is the result of the accumulation of 10 scans at a resolution of 4 cm^{-1}, making it possible to obtain an IR spectrum every 10 s. The gas flows of He, N_2O, and NO were regulated with thermal mass flow controllers.

2.3. Catalytic testing

2.3.1. Parallel reaction setup

Catalytic reaction experiments were performed in an automated 10-flow parallel reactor setup. The reactor beds were contained in a quartz reactor bed with an internal diameter of 4 mm. The catalyst (sieve fraction, 0.25–0.5 mm) was retained between two quartz wool plugs. The standard pretreatment involved preheating at a rate of 1 °C/min to 450 °C (overnight) under a He flow (50 ml/min). The reactions were carried out at 400, 450, and 500 °C. Table 2 gives the compositions of the various reactant feeds for the different reactions. The quartz reactors were placed in a radially heated, temperature-controlled stainless steel oven. The reactant feed (total flow, 1000 ml/min) was composed by mixing appropriate flows of reaction gases through thermal mass flow controllers (Bronkhorst). The total reactant flow was distributed over a set of capillaries placed

Table 2
Overview of experimental conditions

Experiment	N_2O concentration (%)	NO concentration (%)	Total flow (ml/min)
1% N_2O decomposition	1	0	100
0.5% N_2O decomposition	0.5	0	100
0.02% NO-assisted N_2O decomposition	1	0.02	100
0.1% NO-assisted 1% N_2O decomposition	1	0.1	100
0.1% NO-assisted 0.5% N_2O decomposition	0.5	0.1	100
1% NO decomposition	0	1	20

before the catalytic beds with a pressure drop extensively exceeding that of the catalyst bed. For analysis, the effluent gas was connected via a 12-way valve to a mass spectrometer (Balzers Omnistar).

The conversion of N_2O is calculated from the fraction of inlet N_2O as

$$\left[(N_2O_{inlet} - N_2O_{residual})/N_2O_{inlet}\right]. \quad (1)$$

For the NO-assisted N_2O decomposition experiments, care should be taken as NO can be converted into N_2O [6], which could influence the N_2O concentration and thus the above ratio. Therefore, the NO conversion into N_2O was studied under the NO-assisted N_2O conditions (0.1 or 0.02% NO in 100 ml/min at 450 °C in the absence of N_2O, results not shown). Only 8% of the inlet NO was converted into N_2O for CZ-12-0.56; <5% was converted for all other samples under investigation. Hence, the inlet N_2O concentration could increase only from 1 to 1.004 and 1.0008% for the 0.1% and 0.02% NO-assisted N_2O decomposition experiments, respectively; thus, this increase can be neglected. It can be concluded that the conversion can still be calculated from the fraction of inlet N_2O converted, and no contribution of NO should be accounted for in (1).

2.3.2. Operando UV–vis

Cu-ZSM-5 and Cu-MOR catalysts were tested in a plug-flow reactor (i.d. = 8 mm). 0.2 g of the catalyst (pellets of 0.25–0.5 mm) was loaded in the reactor. The standard pretreatment involved preheating at 1 °C/min to 450 °C (overnight) under a He flow (50 ml/min). The reactions were carried out at 400, 450, and 500 °C. The reaction feed was obtained by blending 10 mol% NO in He, 5 mol% N_2O in He, and balance He. Table 2 presents the composition of the inlet gas for the different reactions.

A HP 4890D gas chromatograph (GC) equipped with a packed column (13X) from Varian and a TCD detector was used to monitor on line the concentrations of N_2, O_2, and N_2O in the effluent. Calibration curves for all three gases were constructed to calculate the different concentrations.

For CZ-12-0.56, an operando UV–vis experiment was performed during the direct and NO-assisted N_2O decomposition. The catalyst was continuously monitored by optical fiber UV–vis spectroscopy in the diffuse reflectance mode. The setup consists of a plug-flow reactor fitted inside a furnace, a UV–vis light source (Top Sensor Systems DH-2000 deuterium–halogen light source) and a photodiode array detector (Ocean Optics SD 2000) connected to the catalyst bed via optical fiber technology (Top Sensor Systems FCB-UV400-ME cable and FCB-UV400G-0.1-XHT high-temperature probe). The probe was mounted outside the reactor, and spectra were collected through the quartz reactor wall. Before the experiment, the UV–vis spectrum of a reactor containing hydrated Na-ZSM-5 was recorded, and subsequently all measured Cu-ZSM-5 spectra were subtracted. Typically, one spectrum in the 40,000–12,000 cm^{-1} region is the result of the superposition of 5000 scans, each taking 50 ms [6].

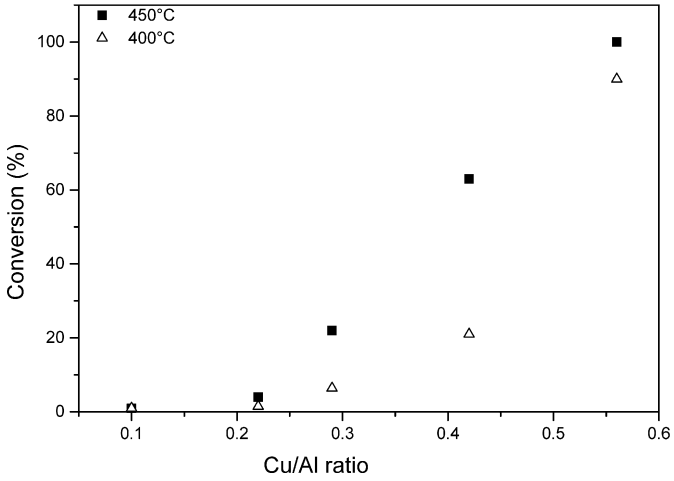

Fig. 1. Conversion of 1% N_2O in He at 450 °C and at 400 °C over Cu-ZSM-5 catalysts as a function of the Cu/Al ratio.

3. Results

3.1. Direct N_2O decomposition

Fig. 1 plots the conversion of N_2O against the Cu/Al ratio for the Cu-ZSM-5 catalysts. At both 400 and 450 °C, a steady increase in conversion is observed with increasing Cu content. For the catalysts with Cu/Al $\leqslant$ 0.22, the conversion is <5%. For Cu/Al > 0.22, the conversion increases steadily to reach for Cu/Al = 0.56 100% at 450 °C and 90% at 400 °C.

Eight other Cu-zeolites were also tested under similar reaction conditions. Table 3 gives the conversions and turnover frequencies (TOFs) for a reaction temperature of 450 °C. From Table 3, it follows that for MFI, MOR and FER, the conversion or TOF is small for Cu/Al $\leqslant$ 0.22, but the TOF increases steadily with the Cu content for catalysts with Cu/Al > 0.22, and that zeolite BEA is much less active than the three others, especially at high Cu loadings. Quite generally, we conclude that MFI (Si/Al = 12)-based catalysts perform best, followed by MOR (Si/Al = 8.8), FER (Si/Al = 6.2), and MOR (Si/Al = 5.3). Cu in zeolite BEA (Si/Al = 9.8) is the least active.

3.2. NO-assisted N_2O decomposition

Table 3 presents the conversion of N_2O in the presence of 0.02% NO and 0.1% NO at 450 °C. For all catalysts, the conversion increases with addition of NO, except for CZ-12-0.56. This

Table 3
Conversion data of direct and NO-assisted N_2O decomposition

Sample	Conversion 1% N_2O at 450 °C (%)	TOF 1% N_2O at 450 °C (h^{-1})	Conversion 0.02% NO-assisted N_2O at 450 °C (%)	Conversion 0.1% NO-assisted N_2O at 450 °C (%)	Conversion 1% NO at 500 °C (%)	TOF 1% NO at 500 °C (h^{-1})
CZ-12-0.56	100	17.5	97	93	55	2.0
CZ-12-0.42	63	16.2	82	88	n.a.	n.a.
CZ-12-0.29	22	7.4	48	62	n.a.	n.a.
CZ-12-0.22	4	1.5	14	20	n.a.	n.a.
CZ-12-0.10	1	0.8	4	7	<1	<0.1
CM-5.3-0.39	32	5.1	57	67	n.a.	n.a.
CM-5.3-0.22	2	0.6	12	17	<1	<0.1
CM-8.8-0.50	61	8.5	76	82	12	0.4
CM-8.8-0.20	2	0.7	12	20	<1	<0.1
CF-6.2-0.42	49	6.3	54	57	9	0.3
CF-6.2-0.21	6	1.4	10	16	<1	<0.1
CB-9.8-0.38	5	1.4	13	22	<1	<0.1
CB-9.8-0.17	1	0.6	7	12	<1	<0.1

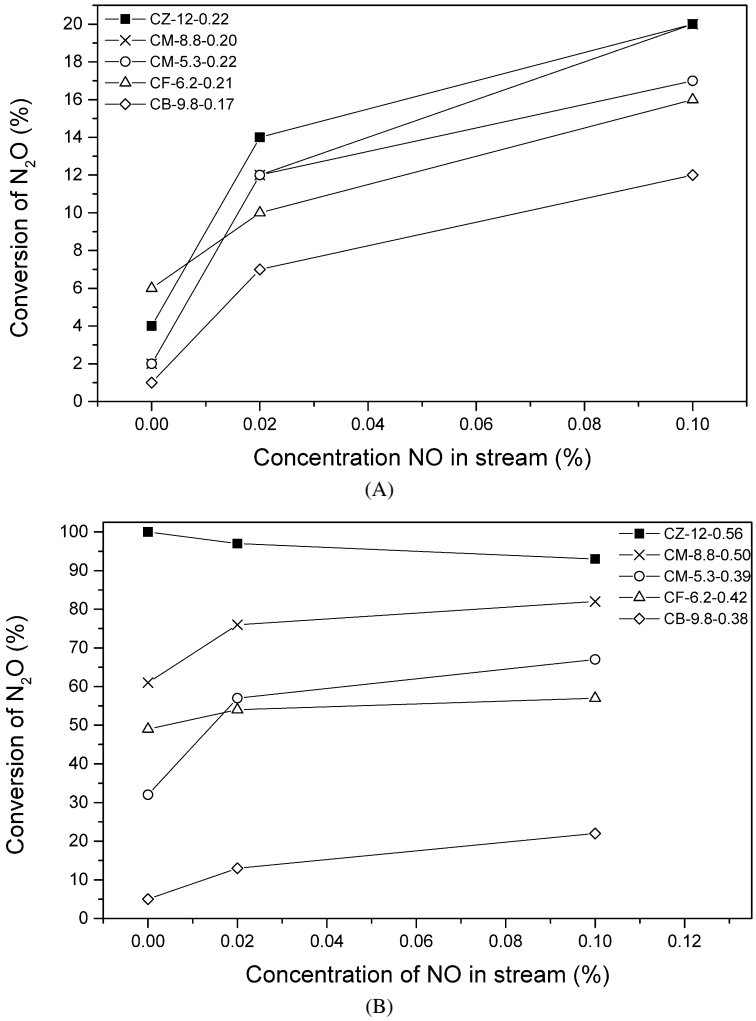

Fig. 2. Conversion of 1% N_2O at 450 °C with increasing amount of NO added for (A) the Cu-zeolites with Cu/Al $\leqslant$ 0.22 and (B) Cu/Al > 0.35.

is shown more clearly in Fig. 2. At low Cu loading (Fig. 2A), the positive effect of NO is most pronounced, irrespective of the zeolite topology. Typically, conversions of 0–5% are increased to 10–15% with 0.02% NO and to 12–20% for 0.1% NO. At high Cu loading (Fig. 2B), the effect of NO is less pronounced, with typical increases in conversion of 5–10%. Only for CZ-12-0.56 is the effect of NO negative. This negative effect was also observed at 400 °C, with conversion dropping from 90 to 86% and 79% in the presence of 0.02% and 0.1% NO, respectively.

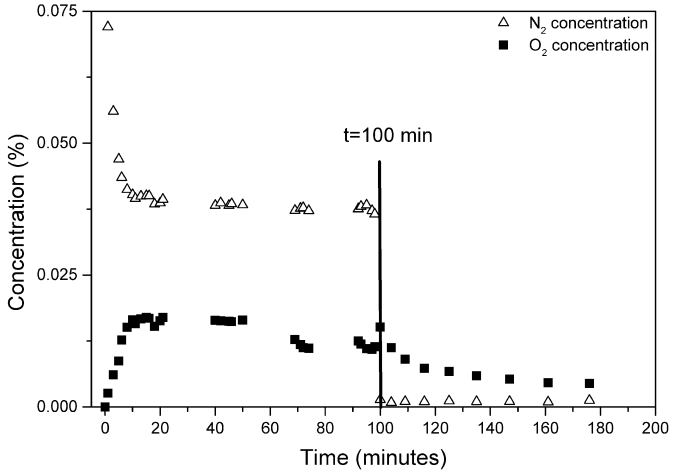

Fig. 3. N_2 and O_2 concentration profiles during 1% NO decomposition at 500 °C as a function of time.

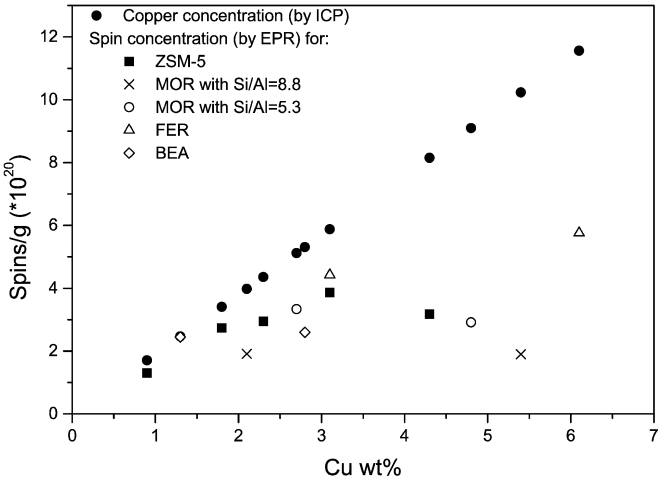

Fig. 4. Amount of spins/g sample detected with EPR compared with the amount of Cu obtained with ICP as a function of the Cu wt%.

3.3. NO decomposition

Catalysts with the highest Cu loading were tested in direct NO decomposition using 1% NO in He at 500 °C; the conversions and TOFs for the different samples are given in Table 3. The activity sequence is CZ12-0.56 > CM-8.8-0.50 > CF-6.2-0.42. The other catalysts tested had TOFs < 0.1.

The amounts of N_2 and O_2 were monitored by GC during the operando UV–vis experiments. The detected N_2 and O_2 concentrations in the reactor outlet are shown in Fig. 3 as a function of time for CM-8.8-0.50. Exposing the catalyst to NO at 500 °C ($t = 0$ min) resulted in an instantaneous increase in N_2 concentration, whereas almost no O_2 was formed. Over time, the N_2 concentration in the outlet decreased, whereas the O_2 concentration increased. After about 10 min, steady-state profiles in N_2 and O_2 were approached. For the NO decomposition, equal amounts of N_2 and O_2 are expected; however, we observed almost twice as much N_2 as O_2. Residual NO likely reacts with O_2 in the cool exit zone of the reactor to NO_2, lowering the amount of O_2 [59]. At $t = 100$ min, the flow was switched back from NO to He. The N_2 concentration in the outlet immediately dropped to zero, whereas the O_2 content in the gas decreased only slowly with time, in good agreement with previously published results on Cu-ZSM-5 [6,60,61]. Repeating these experiments for CF-6.2-0.42 and CZ-12-0.56 resulted in similar N_2 and O_2 profiles (results not shown).

3.4. Spectroscopy

3.4.1. EPR

The EPR spectra of the calcined Cu-zeolites are characterized by two signals due to isolated Cu(II) ions. The characteristic g-values of these signals are $g_{\parallel}^1 = 2.271$ and $g_{\parallel}^2 = 2.314$, in agreement with published EPR spectra [7,62]. With increasing Cu loading comes a growing discrepancy between the amount of Cu(II) determined by chemical analysis and the amount determined by EPR. This difference, called *EPR-silent Cu* (Table 4), is calculated after integrating the entire EPR spectrum and subtracting these values from the total amount of copper as determined by ICP. The data are presented in Fig. 4. Below 2 wt% Cu, there is almost no EPR-silent Cu. At higher Cu content, the EPR-silent fraction increases, due to antiferromagnetic coupling between closely spaced Cu sites [7,62]. Table 4 gives the wt% EPR-silent Cu.

Table 4
Spectroscopic results for the Cu-zeolites

Sample	wt% EPR silent Cu	NO_2/NO band intensity ratio for 0.5% N_2O + 0.02% NO	NO_2/NO band intensity ratio for 0.5% N_2O + 0.1% NO	Average volume available per Cu (Å^3)
CZ-12-0.56	2.6	2.9	2.0	29.4
CZ-12-0.42	1.1	n.a.	n.a.	39.8
CZ-12-0.29	0.8	n.a.	n.a.	53.6
CZ-12-0.22	0.4	7.8	2.5	61.7
CZ-12-0.10	0.2	1.5	0.8	137.1
CM-5.3-0.39	3.3	6.1	2.2	26.7
CM-5.3-0.22	1.0	7.1	2.1	47.5
CM-8.8-0.50	4.4	5.3	2.2	23.7
CM-8.8-0.20	1.1	5.5	1.8	60.9
CF-6.2-0.42	2.9	2.8	1.6	27.2
CF-6.2-0.21	0.9	4.4	1.6	53.6
CB-9.8-0.38	1.4	4.3	1.7	39.3
CB-9.8-0.17	0.0	1.2	0.8	84.7

Dividing the unit cell volume [63] by the total number of Cu atoms per unit cell gives the average volume per Cu atom, assuming a random distribution of the Cu ions. These values for the materials under study are collected in Table 4. Plotting these values against the loadings of EPR-silent Cu (Fig. 5) reveals an almost exponential decay of the volume per Cu atom with an increasing amount of EPR-silent Cu, irrespective of the zeolite topology. A volume of 35 Å^3 appears to be a threshold separating low (<1.5 wt%) and high (>2.5 wt%) amounts of EPR-silent Cu.

3.4.2. FTIR

The FTIR spectra of the NO-assisted N_2O decomposition are displayed in Fig. 6. A blank experiment of 0.5% N_2O + 0.1% NO in He over Na-ZSM-5 at 450 °C, in which only gas

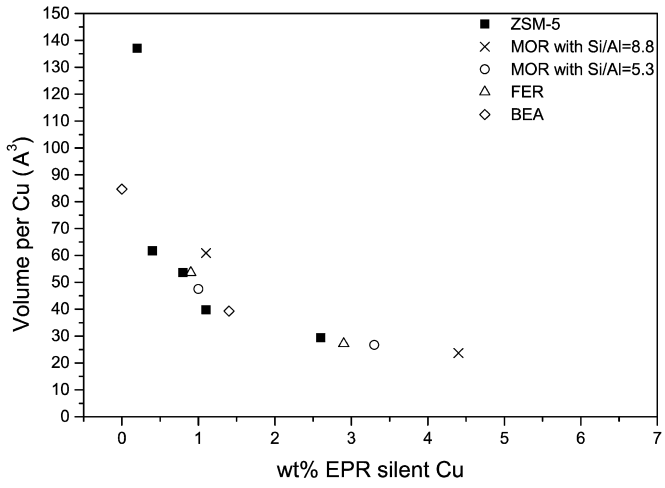

Fig. 5. Average volume available per Cu atom as a function of the absolute amount of EPR silent Cu atoms present.

phase molecules were observed, is shown in Fig. 6A. The absorption bands have an unresolved rotational fine structure, leading to doublets. The doublets at 2580/2550, 2478/2443, and 2236/2213 cm^{-1} are assigned to gaseous N_2O [47], whereas the doublet at 1908/1846 cm^{-1} is due to gaseous NO. The doublet at 2360/2337 cm^{-1} was visible both during N_2O and NO treatment and might be due to small traces of CO_2 located outside the reaction cell.

Fig. 6B shows the time evolution of the FTIR spectra for CM-8.8-0.50. At 300 °C, after switching from a 0.5% N_2O/He to a 0.1% NO/He flow, the immediate formation of bands at 1625, 1598, and 1572 cm^{-1}, assigned to sorbed NO_2 and NO_3 species (hereinafter referred to as NO_x), was observed [64–70]. Similar sorbed NO_x species were detected for all Cu-containing zeolites. Switching from a He flow to the 0.1% NO flow at 300 °C did not result in the formation of these infrared adsorption bands, suggesting that the sorbed NO_x species result from a reaction between NO molecules and extra-lattice oxygen (ELO)

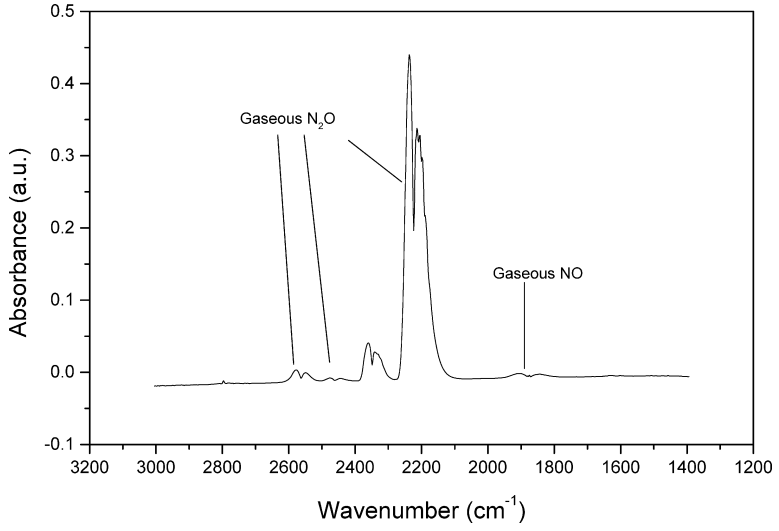

(A)

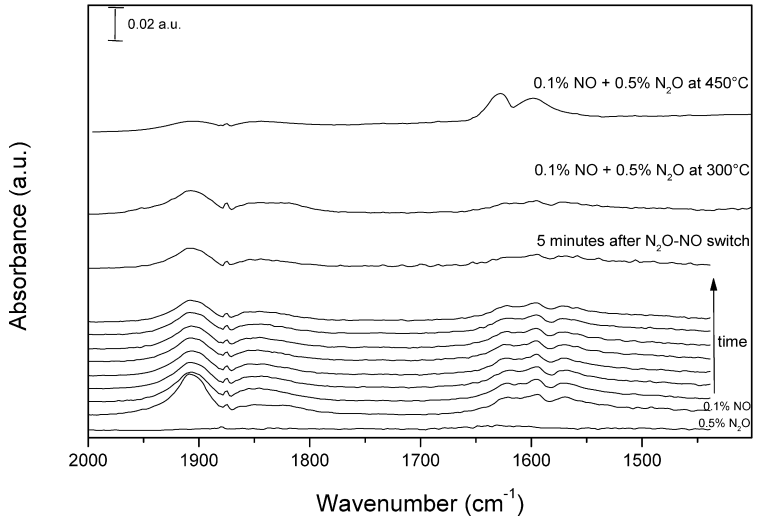

(B)

Fig. 6. FTIR spectra of (A) Na-ZSM-5 during 0.5% N_2O + 0.1% NO treatment at 450 °C and (B) CM-8.8-0.50 after switching from a 0.5% N_2O/He to a 0.1% NO/He flow at 300 °C and during 0.1% NO + 0.5% N_2O treatment at 300 and 450 °C.

atoms deposited by N_2O. Once formed, the NO_x species slowly disappear with time. After 5 min, the bands have almost fully disappeared, indicating that these NO_x species slowly decompose at 300 °C. Switching from 0.1% NO/He to 0.5% N_2O/He did not accelerate the decomposition of these bands, indicating that no reaction of sorbed NO_x with N_2O occurred, as was proposed in one of the mechanisms for low-loaded Fe-ZSM-5 [49]. The NO_x species autodesorb.

Fig. 6B shows an FTIR spectrum obtained during 0.1% NO + 0.5% N_2O treatment at 300 °C. The presence of sorbed NO_x species can still be observed. The IR bands of the adsorbed NO_x species are weak but constant over time. This suggests that a steady-state situation of formation and decomposition of sorbed NO_x species is attained at 300 °C. This results in low decomposition of N_2O, because small traces of N_2 were detected during the 0.1% NO + 0.5% N_2O reaction at 300 °C. Nitrogen was not observed during treatment with 0.5% N_2O at 300 °C.

Increasing the temperature to 450 °C during the 0.1% NO + 0.5% N_2O treatment results in loss of the bands attributed to the sorbed NO_x species, but new bands at 1630 and 1599 cm^{-1} assigned to gaseous NO_2 appear for all Cu samples (Fig. 6B). Because it is known from the literature that adsorbed NO_x species are not stable at this temperature, it is not surprising that only gaseous species are observed and (intermediate) adsorbed species are no longer visible [68,69].

In blank experiments with mixtures of 0.5% N_2O + 1% O_2 + 0.1% or 0.02% NO over Na-ZSM-5 at 450 °C, only gaseous NO_2 (1599–1630 cm^{-1}) and gaseous NO (1847–1905 cm^{-1}) were observed [71]. The ratio of the IR band intensities $I(NO_2)/I(NO)$ was 0.5 and independent of the initial amount of NO. Although thermodynamic equilibrium might not yet have been attained, this ratio can be considered the result of the noncatalyzed gas-phase reaction

$$2NO + O_2 \leftrightarrows 2NO_2.$$

Table 4 presents the $I(NO_2)/I(NO)$ band intensity ratios for the Cu-zeolites during both 0.5% N_2O + 0.02% NO and 0.5% N_2O + 0.1% NO reactions. Comparing these ratios with the ratio of 0.5 from the blank experiments with Na-ZSM-5 clearly shows that an excess amount of NO_2 was formed over all Cu-zeolites at 450 °C for both gas compositions. For the 0.02% NO mixture, $I(NO_2)/I(NO)$ ratios up to 7.8 were observed, which is about 15 times higher than the ratio observed in the Cu-free experiment. Increasing the NO concentration in the feed from 0.02 to 0.1% resulted in an increased intensity in both the NO_2 and NO signals but a decrease in the $I(NO_2)/I(NO)$ ratio. However, in all cases the ratio remained significantly >0.5.

3.4.3. UV–vis

An operando UV–vis study was performed on the CZ-12-0.56 sample. Fig. 7 shows a UV–vis spectrum of the catalyst during N_2O decomposition at 450 °C. The typical band of the bis(μ-oxo)dicopper core is seen at 22,000 cm^{-1} [9,10]. The intensity of this band decreases for the NO-assisted N_2O decomposition reaction, indicating some decomposition of the complex with NO. Presumably, NO picks up O atoms to form NO_2.

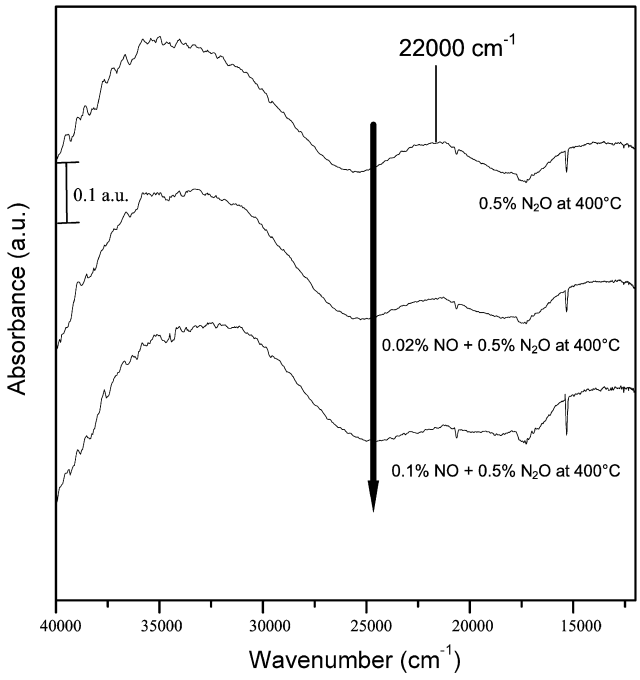

Fig. 7. UV–vis spectra of CZ-12-0.56 during 0.5% N_2O decomposition and 0.1 and 0.02% NO-assisted N_2O decomposition at 400 °C.

4. Discussion

4.1. Direct NO and N_2O decomposition

Our previous research on the catalytic decomposition of NO and N_2O over Cu-MFI zeolites revealed that the bis(μ-oxo)dicopper core is the key intermediate, allowing for the controlled release of O_2 [6,7]. This core is also the key intermediate in the selective oxidation of methane into methanol at temperatures as low as 115 °C [9]. The optimal catalyst contains a relatively high amount of Cu (Cu/Al > 0.22) and Si/Al ratios of 12–30. The same dicopper core was identified in Cu-exchanged mordenite, although in much smaller amounts. Cu-exchanged FER and BEA do not contain such bis(μ-oxo)dicopper core irrespective of the Cu loading and are inactive in the selective oxidation of CH_4 at 115 °C. However, at higher temperatures (200 °C), methanol could be formed, which is indicative of the presence of other active Cu species [10].

In the present study, MFI, MOR, FER, and BEA structures were systematically investigated in the catalytic decomposition of N_2O and NO. From Table 3, the following activity series can be discerned for the samples with high Cu loading (Cu/Al $\geqslant$ 0.29): MFI > MOR with Si/Al = 8.8 > FER > MOR with Si/Al = 5.3. Highly loaded Cu-BEA (CB-9.8-0.38) and samples with low Cu loading (Cu/Al $\leqslant$ 0.22) show little activity.

Samples with Cu/Al $\geqslant$ 0.29 typically contain EPR-silent Cu, the amount of which increases with Cu loading (Table 4). EPR-silent Cu species originate from an antiferromagnetic interaction of Cu^{2+} with other species. These interactions are likely due to the close proximity of other Cu^{2+} species [7]. Fig. 8 shows the TOF as a function of the amount of EPR-silent Cu. Based on this figure, the following observations can

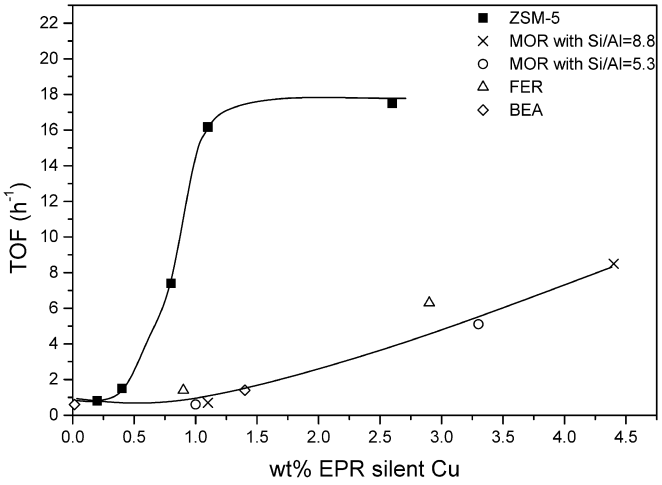

Fig. 8. TOF of N_2O decomposition (1% N_2O in He) at 450 °C as a function of the amount of EPR silent Cu in the different Cu-zeolites.

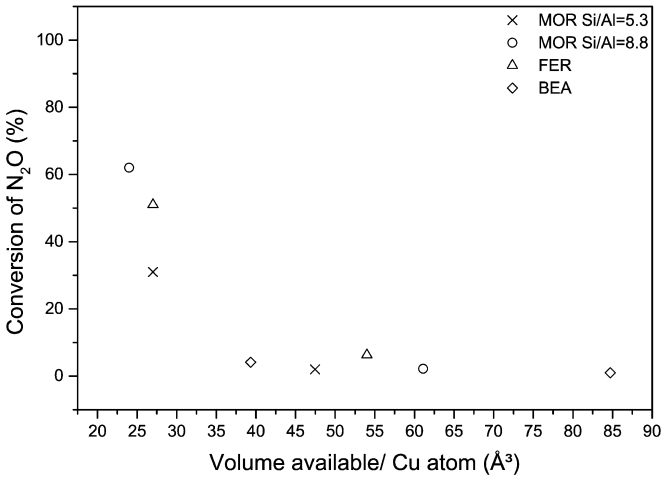

Fig. 9. Conversion of 1% N_2O at 450 °C as a function of volume/Cu atom in the MOR, FER and *BEA samples.

be made: (1) In the ZSM-5 series, a sudden increase of TOF for CZ-12-0.29 (i.e., >0.5 wt% EPR-silent Cu) was observed; (2) MOR, FER, and BEA samples showed a smooth increase in TOF with the amount of EPR-silent Cu; (3) and samples with low EPR-silent Cu content had low TOF irrespective of the zeolite structure.

This typical behavior can be interpreted qualitatively given our present knowledge of the active sites. In the Cu-ZSM-5 series at Cu/Al > 0.22, increasing amounts of bis(μ-oxo)dicopper cores were formed with increasing Cu/Al ratios [9]. In line with our previous reports on Cu-ZSM-5 [6,7], the sudden increase in TOF at CZ-12-0.29 is attributed to the increasing number of bis(μ-oxo)dicopper cores. As Fig. 8 shows, the activity of this core exceeds that of the active sites in the other Cu-zeolites under investigation. In MOR and FER, the active sites have not yet been identified; however, the relation in Fig. 8 suggests that the active sites contain EPR-silent Cu. The low activities of CB-9.8-0.38 and of the samples with low Cu loading (Cu/Al $\leqslant$ 0.22), independent of the zeolite topology, can be understood based on the low amounts of EPR-silent Cu.

Because EPR-silent copper likely relates to the proximate presence of other Cu species, the average volume per Cu atom in each zeolite was determined assuming a random distribution of Cu throughout the zeolite crystal. Fig. 9 plots the conversion versus this parameter for the MOR, FER and BEA samples. Above a Cu volume of 35 Å^3, the conversion is essentially zero, independent of the zeolite topology. Smaller volumes result in an exponential increase in conversion. Although deviation from random Cu distribution might result in smaller Cu–Cu distances, due to, e.g., site preference of Cu^{2+} [62,72], or the formation of bis(μ-oxo)dicopper cores [7–10] or chain-like $(Cu–O–)_n$ species at high Cu loading [73], this parameter can be used as an easy approach to predict whether high activity in the direct N_2O decomposition for a Cu-zeolite can be expected. A spherical volume of 35 Å^3 corresponds to a Cu–Cu distance of 4.1 Å. This implies that for Cu–Cu distances <4.1 Å, the activity in the direct N_2O decomposition is high. The fact that the bis(μ-oxo)dicopper core, characterized by a Cu–Cu distance of about 2.9 Å [7], is the most active site for the N_2O decomposition further emphasizes the importance of the Cu–Cu distance.

Oxygen–oxygen recombination is known to be the rate-limiting step in N_2O decomposition [20,43–51,67,74–76]. The role of the active site is to abstract oxygen atoms from N_2O. These oxygen atoms then migrate over the catalyst surface and eventually recombine to O_2, which desorbs. A large distance between the abstracted oxygen atoms decreases the rate of recombination to molecular oxygen [45,47]. This situation arises for low Cu loadings and in situations in which the amount of EPR-silent Cu is low. The fact that decreasing Cu–Cu distances results in increases in both the amount of EPR-silent Cu atoms and TOF demonstrates that oxygen–oxygen recombination is facilitated by these smaller Cu–Cu distances. In the limit, with the presence of the bis(μ-oxo)dicopper core, O_2 migration is not necessary, because two O atoms are incorporated in the same dinuclear Cu center. The difference in the migration of oxygen thus explains the observed activity series for the N_2O decomposition: bis(μ-oxo)dicopper cores > other EPR-silent Cu sites > isolated, EPR-active Cu sites.

The importance of closely located Cu sites is also shown in the catalytic decomposition of NO. From Table 3, the same activity order as for the direct N_2O decomposition can be discerned. The N_2 and O_2 concentration profiles observed during opening and closing of the NO flow (Fig. 3) confirm that for NO decomposition, recombinative O_2 desorption is the rate-determining step [7,77]. At the initial stage of the reaction, NO is decomposed on vacant Cu sites, resulting in N_2 and adsorbed O atoms. As time proceeds, the surface becomes saturated with deposited O atoms, resulting in a decrease of the NO decomposition activity and a lowered N_2 concentration at the outlet. At the same time, O atoms start recombining to form molecular oxygen and creating vacant Cu sites. After 10 min, a steady state is approached. On closing the NO flow ($t = 100$ min), N_2 formation stops immediately. However, Cu–O species are still present at the surface, as is evident from the continuing desorption of molecular oxygen.

4.2. NO-assisted N_2O decomposition

Moulijn and co-workers [43,51] and Sang et al. [49,50] presented several possible pathways for the NO-promoting effect on the decomposition of N_2O over Fe-zeolites. Generally, two mechanisms for the positive effect of NO have been put forward. In the first of these, NO temporarily stores oxygen atoms in the form of adsorbed NO_x molecules, thereby freeing the active site for a second N_2O molecule. A second oxygen atom is deposited, which then recombines with the stored oxygen atom to molecular oxygen. An alternative is the enhanced migration of oxygen over the catalytic surface via NO_x intermediates either at the surface or via the gas phase. As a consequence, the rate of recombination is increased. Thus, NO is used as a storage or transport medium for oxygen atoms, facilitating the recombination of two oxygen atoms. The role of NO as oxygen carrier also has been reported for the NO decomposition over Cu-ZSM-5 [14,60].

An infrared study of our Cu samples has shown (Fig. 6B) that NO scavenges O atoms deposited by N_2O. This results in adsorbed NO_x at 300 °C and gaseous NO_2 at 450 °C. After desorption of NO_2, vacant Cu sites are regenerated that can accept a new O atom from another N_2O molecule. The liberation and reoxidation of the Cu sites at 300 °C was confirmed during the catalytic experiments. At 450 °C, it is reported [68,69] that the NO_x species are no longer stable and quickly desorb. This explains the observed increase in NO_2 formation in the gas phase. In addition, following the typical charge-transfer band of the bis(μ-oxo)dicopper core with operando UV–vis spectroscopy (Fig. 7) shows that introducing NO leads to the abstraction of bridging oxygen species.

On the addition of NO, the rate of nitrous oxide decomposition increases, leading to increased concentrations of nitrogen and oxygen (except for CZ-12-0.56). This implies that NO acts as a catalytic species and that not only a stoichiometric reaction between NO and N_2O occurs. (If that were the case, then only an increased amount of N_2 would be observed.) Further evidence for the catalytic effect of NO rather than a stoichiometric reaction comes from the observation that the extra amount of N_2O decomposed is several times higher than the amount of NO added. For example, over CM-5.3-0.39, an additional 0.25% N_2O is decomposed on introduction of 0.02% NO.

Based on the above observations, the following mechanism is presented to explain the NO-assisted N_2O decomposition over the Cu-zeolites (Scheme 1). First N_2O is decomposed to molecular nitrogen and an oxygen atom is deposited on vacant Cu sites, thereby creating a Cu–O species (1). NO scavenges this oxygen, creating sorbed NO_x species at 300 °C or gaseous NO_2 molecules at 450 °C (2). Finally, gaseous NO_2 molecules release O_2 either via a reaction with a second deposited oxygen atom (3′, Scheme 1A) or via the thermodynamically driven gaseous reaction of two NO_2 molecules (3″, Scheme 1B).

Infrared measurements during the NO-assisted N_2O decomposition at 450 °C show that large amounts of NO_2 are formed (Fig. 6B) that were not observed in a blank experiment with Na-ZSM-5. This not only proves that NO_2 is an intermediate in the NO-assisted N_2O decomposition, but also indicates that

$$
\begin{aligned}
&(1)\ 2N_2O + 2Cu^* \rightarrow 2N_2 + 2Cu\text{–}O\\
&(2)\ Cu\text{–}O + NO \rightarrow Cu\text{–}NO_x \text{ (at 300 °C)}\\
&\qquad\qquad Cu^* + NO_2 \text{ (at 450 °C)}\\
&(3')\ NO_2 + Cu\text{–}O \rightarrow Cu^* + NO + O_2\\
&\text{Overall: } 2N_2O \rightarrow 2N_2 + O_2\\
&\qquad\qquad\qquad (A)
\end{aligned}
$$

$$
\begin{aligned}
&(1)\ 2N_2O + 2Cu^* \rightarrow 2N_2 + 2Cu\text{–}O\\
&(2)\ 2Cu\text{–}O + 2NO \rightarrow 2Cu\text{–}NO_x \text{ (at 300 °C)}\\
&\qquad\qquad 2Cu^* + 2NO_2 \text{ (at 450 °C)}\\
&(3'')\ 2NO_2 \rightarrow 2NO + O_2\\
&\text{Overall: } 2N_2O \rightarrow 2N_2 + O_2\\
&\qquad\qquad\qquad (B)
\end{aligned}
$$

Scheme 1. Reaction pathways for the NO-assisted N_2O decomposition.

the rate of the NO-assisted N_2O decomposition is controlled by the $NO_2 \rightarrow NO$ conversion, as was also reported for Fe-zeolites [45].

For all of the Cu-zeolites under investigation, $I(NO_2)/I(NO)$ ratios higher than the ratio obtained in the blank experiments are observed. This suggests that the mechanism presented in Scheme 1 holds for all Cu sites: NO does not distinguish between the oxygen atoms at EPR-silent or isolated EPR-detectable Cu sites. However, the influence on the overall activity does differ. Table 3 shows that isolated, EPR-detectable Cu sites benefit the most from the addition of NO. At the EPR-silent Cu sites, the effect of NO is still positive, although to a much lesser extent, to become even negative at the bis(μ-oxo)dicopper core, as can be seen from the decrease of conversion in CZ-12-0.56 (Fig. 2B).

The observed difference can be explained by the mechanism of the NO-assisted N_2O decomposition. NO acts as a transport agent for oxygen atoms deposited on Cu sites. When the distance between these Cu sites is large (i.e., at low Cu loading or EPR-detectable Cu sites), this gas-phase transport significantly accelerates oxygen migration. At decreasing Cu–Cu distances, oxygen recombination is accelerated, because good activity was already observed in the direct N_2O decomposition. No further acceleration of the migration step is obtained by adding NO. Therefore, the beneficial effect of NO is no longer as pronounced as for the isolated Cu sites. Oxygen migration over several atoms is not necessary at the bis(μ-oxo)dicopper core. An operando UV–vis study clearly proved that NO abstracts oxygen atoms from this core, because the intensity of the characteristic charge-transfer band at 22,700 cm^{-1} decreases. In this way, an additional step is created that slows down the recombination of oxygen atoms and results in an overall negative effect in CZ-12-0.56.

4.3. Cu-ZSM-5 versus Fe-ZSM-5

In Fe-ZSM-5, both fast and slow O_2 desorption pathways were observed during the direct N_2O decomposition. The fast pathway was assigned to the recombination of two oxygen atoms, deposited in close vicinity, whereas the slow desorption pathway was associated with migration of the oxygen atoms over the catalyst surface. Both pathways contribute to the steady-state activity, as reported by Pirngruber and co-workers [16,76,78]. Although it is often reported that the activity of the

Fe species in Fe-ZSM-5 strongly depends on the preparation method, their different catalytic behavior can be attributed to a different contribution to the fast or slow O_2 desorption process [16,79–85].

In the Cu-exchanged zeolites under investigation, similar observations as for Fe-ZSM-5 were made; the distance between deposited O atoms strongly influences O migration and hence the O_2 desorption rate. As the average Cu–Cu distance drops below 4.1 Å, oxygen migration and recombination becomes fast. At the bis(μ-oxo)dicopper cores in Cu-ZSM-5, however, O-migration is not necessary, because two O atoms are present in the bis(μ-oxo)dicopper core (O–O distance of 2.3 Å was reported [86]). This greatly facilitates oxygen recombination.

In both Fe- and Cu-zeolites, NO acts as a transport or storage medium for O atoms, thereby creating a faster pathway for oxygen migration [43–53]. The difference between Cu-ZSM-5 and Fe-zeolites is the stabilization of the bis(μ-oxo)dicopper core. Whereas some have reported similar binuclear Fe-sites in Fe-ZSM-5 [54,87–95], only one extra lattice oxygen is incorporated into this core to the best of our knowledge [54,91,94,95]. Therefore, O migration is still necessary in Fe-ZSM-5. This is not the case for Cu-ZSM-5, containing the bis(μ-oxo)dicopper core. Therefore, the latter is responsible for the superior activity of Cu-ZSM-5, as is often reported [33,96,97].

5. Conclusion

Cu-exchanged zeolites were investigated in the direct decomposition of N_2O and NO. TOF of the catalysts are related to the amount of EPR-silent copper. Two types of active sites are present: the bis(μ-oxo)dicopper core in ZSM-5 zeolites and not yet identified EPR-silent Cu species in highly loaded (Cu/Al $\geqslant$ 0.29) MOR and FER. The former is much more active than the latter. This can be explained by the rate-limiting step: oxygen–oxygen recombination into molecular oxygen. In the bis(μ-oxo)dicopper core, the two oxygen atoms can recombine without migration over the surface. In the zeolites with not-yet identified EPR-silent Cu species, oxygen atom migration precedes recombination, the rate of which is strongly dependent on the average distance between Cu atoms. In CB-9.8-0.38 and the samples with low Cu loading (Cu/Al $\leqslant$ 0.22), this distance is too large, hindering the recombination of oxygen atoms. Hence the low activity of these samples is understood.

NO has a positive effect on the N_2O decomposition in all samples tested except for the ZSM-5 sample with the highest Cu loading (CZ-12-0.56). NO scavenges the oxygen atoms deposited by N_2O to form adsorbed NO_x at 300 °C and gaseous NO_2 at 450 °C. Thereby vacant Cu sites are regenerated, which can accept another oxygen from N_2O. The addition of NO also influences the migration rate of oxygen atoms as oxygen atoms travel through the gas phase as $(NO_2)_{gas}$. The largest positive effect of NO was observed for the isolated, EPR-detectable sites. Because NO also scavenges bridging oxygen atoms from the bis(μ-oxo)dicopper core, an additional migration step is created, slowing down the oxygen–oxygen recombination. This explains the observed negative effect of NO on the bis(μ-oxo)-dicopper cores in ZSM-5.

Acknowledgments

P.J.S. thanks the Institute for the Promotion of Innovation by Science and Technology in Flanders (IWT-Vlaanderen) for a research grant. M.H.G. thanks the Fund for Scientific Research-Flanders (FWO-Vlaanderen) for a postdoctoral fellowship. This investigation was supported by grants from FWO-Vlaanderen, the Concerted Research Action (GOA), and the Interuniversity Attraction Pool (IAP) program.

References

[1] M. Iwamoto, H. Yahiro, K. Tanda, N. Mizuno, Y. Mine, S. Kagawa, J. Phys. Chem. 95 (1991) 3727.
[2] G. Centi, S. Perathoner, Appl. Catal. A 132 (1995) 179.
[3] E. Jobson, Microporous and mesoporous materials as catalytic hosts for Fe, Co and Cu, international workshop organized by the DZA, Scheveningen, The Netherlands, 1–4 March 2005, paper P6.
[4] H. Yahiro, M. Iwamoto, Appl. Catal. A 222 (2001) 163.
[5] Y. Kuroda, M. Iwamoto, Top. Catal. 28 (2004) 111.
[6] M.H. Groothaert, K. Lievens, H. Leeman, B.M. Weckhuysen, R.A. Schoonheydt, J. Catal. 220 (2003) 500.
[7] M.H. Groothaert, J.A. van Bokhoven, A.A. Battiston, B.M. Weckhuysen, R.A. Schoonheydt, J. Am. Chem. Soc. 125 (2003) 7692.
[8] M.H. Groothaert, K. Lievens, J.A. van Bokhoven, A.A. Battiston, B.M. Weckhuysen, K. Pierloot, R.A. Schoonheydt, ChemPhysChem 4 (2003) 626.
[9] M.H. Groothaert, P.J. Smeets, B.F. Sels, P.A. Jacobs, R.A. Schoonheydt, J. Am. Chem. Soc. 127 (2005) 1394.
[10] P.J. Smeets, M.H. Groothaert, R.A. Schoonheydt, Catal. Today 110 (2005) 303.
[11] J. Pérez-Ramirez, Patent WO047960A1 (2004), to Norsk Hydro asa.
[12] C. Hamon, K. Malefant, B. Neveu, Patent WO9934901A1 (1999), to Grande Paroisse s.a. and Institut Régional de Matériaux Avancés IRMA.
[13] K. Krishna, M. Makkee, Catal. Lett. 106 (2006) 183.
[14] B. Modén, P. Da Costa, B. Fonfé, D.K. Lee, E. Iglesia, J. Catal. 209 (2002) 75.
[15] M.Y. Kustova, S.B. Rasmussen, A.L. Kustov, C.H. Christensen, Appl. Catal. B 67 (2006) 60.
[16] G.D. Pirngruber, M. Luechinger, P.K. Roy, A. Cecchetto, P. Smirniotis, J. Catal. 224 (2004) 429.
[17] J. Dedecek, O. Bortnovsky, A. Vondrová, B. Wichterlová, J. Catal. 200 (2001) 160.
[18] J. Dedecek, J. Cejka, B. Wichterlová, Appl. Catal. B 15 (1998) 233.
[19] A.T. Bell, Catal. Today 38 (1997) 151.
[20] D.A. Bulushev, L. Kiwi-Minsker, A. Renken, J. Catal. 222 (2004) 389.
[21] R.S. da Cruz, A.J.S. Mascarenhas, H.M.C. Andrade, Appl. Catal. B 18 (1998) 223.
[22] E.J.M. Hensen, Q. Zhu, M.M.R.M. Hendrix, A.R. Overweg, P.J. Kooyman, M.V. Sychev, R.A. van Santen, J. Catal. 221 (2004) 560.
[23] N.W. Cant, I.O.Y. Liu, Catal. Today 63 (2000) 133.
[24] C. He, K. Köhler, Phys. Chem. Chem. Phys. 8 (2006) 898.
[25] Q. Zhu, R.M. van Teeffelen, R.A. van Santen, E.J.M. Hensen, J. Catal. 221 (2004) 575.
[26] H. Imai, T. Ogawa, K. Sugimoto, M. Kataoka, Y. Tanaka, T. Ono, Appl. Catal. B 55 (2005) 259.
[27] C. Resini, T. Montanari, L. Nappi, G. Bagnasco, M. Turco, G. Busca, F. Bregani, M. Notaro, G. Rocchini, J. Catal. 214 (2003) 179.
[28] T. Chaki, M. Arai, T. Ebina, M. Shimokawabe, J. Mol. Catal. A 227 (2005) 187.
[29] M. Yoshida, T. Nobukawa, S. Ito, K. Tomishige, K. Kunimori, J. Catal. 223 (2004) 454.
[30] M. Schwidder, M. Santhosh Kumar, K. Klementiev, M.M. Pohl, A. Brückner, W. Grünert, J. Catal. 231 (2005) 314.
[31] M. Santhosh Kumar, M. Schwidder, W. Grünert, U. Bentrup, A. Brückner, J. Catal. 239 (2006) 173.

[32] T. Nobukawa, M. Yoshida, S. Kameoka, S. Ito, K. Tomishige, K. Kunimori, Catal. Today 93–95 (2004) 791.
[33] D. Kaucký, A. Vondrová, J. Dedecek, B. Wichterlová, J. Catal. 194 (2000) 318.
[34] H. Sjövall, L. Olsson, E. Fridell, R.J. Blint, Appl. Catal. B 64 (2006) 180.
[35] B. Neveu, G. Delahay, M. Mauvezin, B. Coq, Patent WO0048715 (2000), to Grande Paroisse s.a.
[36] A. Guzmán-Vargas, G. Delahay, B. Coq, Appl. Catal. B 42 (2003) 369.
[37] R.Q. Long, R.T. Yang, J. Catal. 188 (1999) 332.
[38] K. Krishna, G.B.F. Seijger, C.M. van den Bleek, M. Makkee, G. Mul, H.P.A. Calis, Catal. Lett. 86 (2003) 121.
[39] G. Busca, M.A. Larrubia, L. Arrighi, G. Ramis, Catal. Today 107–108 (2005) 139.
[40] J. Park, H.J. Park, J.H. Baik, I. Nam, C. Shin, J. Lee, B.K. Cho, S.H. Oh, J. Catal. 240 (2006) 47.
[41] L. Xu, R.W. McCabe, R.H. Hammerle, Appl. Catal. B 39 (2002) 51.
[42] C.A. Jones, D. Stec, S.C. Larsen, J. Mol. Catal. A 212 (2004) 329.
[43] J. Pérez-Ramírez, F. Kapteijn, G. Mul, J.A. Moulijn, J. Catal. 208 (2002) 211.
[44] J. Pérez-Ramírez, G. Mul, F. Kapteijn, J.A. Moulijn, Kinet. Catal. 44 (2003) 639.
[45] D. Kaucký, Z. Sobalík, M. Schwarze, A. Vondrová, B. Wichterlová, J. Catal. 238 (2006) 293.
[46] I. Melián-Cabrera, C. Mentruit, J.A.Z. Pieterse, R.W. van den Brink, G. Mul, F. Kapteijn, J.A. Moulijn, Catal. Commun. 6 (2005) 301.
[47] G.D. Pirngruber, J.A.Z. Pieterse, J. Catal. 237 (2006) 237.
[48] J.A.Z. Pieterse, G. Mul, I. Melian-Cabrera, R.W. Brink, Catal. Lett. 99 (2005) 41.
[49] C. Sang, B.H. Kim, C.R.F. Lund, J. Chem. Phys. B 109 (2005) 2295.
[50] C. Sang, C.R.F. Lund, Catal. Lett. 73 (2001) 73.
[51] G. Mul, J. Pérez-Ramírez, F. Kapteijn, J.A. Moulijn, Catal. Lett. 77 (2001) 7.
[52] M. Kögel, B.M. Abu-Zied, M. Schwefer, T. Turek, Catal. Commun. 2 (2001) 273.
[53] X. Xu, H. Xu, F. Kapteijn, J.A. Moulijn, Appl. Catal. B 53 (2004) 265.
[54] K.A. Dubkov, N.S. Ovanesyan, A.A. Shteinman, E.V. Starokon, G.I. Panov, J. Catal. 207 (2002) 341.
[55] E.J.M. Hensen, Q. Zhu, R.A.J. Janssen, P.C.M.M. Magusin, P.J. Kooyman, R.A. van Santen, J. Catal. 233 (2005) 123.
[56] E.J.M. Hensen, Q. Zhu, R.A. van Santen, J. Catal. 233 (2005) 136.
[57] B.M. Weckhuysen, R.A. Schoonheydt, in: B.M. Weckhuysen, P. Van Der Voort, G. Catana (Eds.), Spectroscopy of Transition Metal Ions on Surfaces, Leuven University Press, Leuven, 2000, p. 25.
[58] B. Schoofs, J.A. Martens, P.A. Jacobs, R.A. Schoonheydt, J. Catal. 183 (1999) 355.
[59] Y.J. Li, W.K. Hall, J. Phys. Chem. 94 (1990) 6145.
[60] B. Modén, P. Da Costa, D.K. Lee, E. Iglesia, J. Phys. Chem. B 106 (2002) 9633.
[61] Z. Schay, H. Knözinger, L. Guczi, G. Pal-Borbély, Appl. Catal. B 18 (1998) 263.
[62] M.H. Groothaert, K. Pierloot, A. Delabie, R.A. Schoonheydt, Phys. Chem. Chem. Phys. 5 (2003) 2135.
[63] W.M. Meier, D.H. Olson, C. Baerlocher, Atlas of Zeolite Structure Types, Elsevier, London, 1996, p. 62.
[64] A.W. Aylor, S.C. Larsen, J.A. Reimer, A.T. Bell, J. Catal. 157 (1995) 592.
[65] T. Cheung, S.K. Bhargava, M. Hobday, K. Foger, J. Catal. 158 (1996) 301.
[66] C. Henriques, M.F. Ribeiro, C. Abreu, D.M. Murphy, F. Poignant, J. Saussey, J.C. Lavalley, Appl. Catal. B 16 (1998) 79.
[67] S. Bennici, A. Gervasini, Appl. Catal. B 62 (2006) 336.
[68] K. Hadjiivanov, D. Klissurski, G. Ramis, G. Busca, Appl. Catal. B 7 (1996) 251.
[69] J. Despres, M. Koebel, O. Kröcher, M. Elsener, A. Wokaun, Micropor. Mesopor. Mater. 58 (2003) 175.
[70] P.T. Fanson, M.W. Stradt, W.N. Delgass, J. Lauterbach, Catal. Lett. 77 (2001) 15.
[71] K. Nakamoto, Infrared and Raman Spectra of Inorganic and Coordination Compounds, Part A, Wiley & Sons, New York, 1997, p. 162.
[72] A. Delabie, K. Pierloot, M.H. Groothaert, B.M. Weckhuysen, R.A. Schoonheydt, Phys. Chem. Chem. Phys. 4 (2002) 134.
[73] S.A. Yashnik, Z.R. Ismagilov, V.F. Anufrienko, Catal. Today 110 (2005) 310.
[74] A. Dandekar, M.A. Vannice, Appl. Catal. B 22 (1999) 179.
[75] D.A. Bulushev, A. Renken, L. Kiwi-Minsker, J. Phys. Chem. B 110 (2006) 305.
[76] G.D. Pirngruber, J. Catal. 219 (2003) 456.
[77] Y.J. Li, W.K. Hall, J. Catal. 129 (1991) 202.
[78] P.K. Roy, G.D. Pirngruber, J. Catal. 227 (2004) 164.
[79] J. Pérez-Ramírez, F. Kapteijn, A. Brückner, J. Catal. 218 (2003) 234.
[80] B.R. Wood, J.A. Reimer, A.T. Bell, M.T. Janicke, K.C. Ott, J. Catal. 224 (2004) 148.
[81] L. Kiwi-Minsker, D.A. Bulushev, A. Renken, J. Catal. 219 (2003) 273.
[82] G.D. Pirngruber, P.D. Roy, Catal. Lett. 93 (2004) 75.
[83] A.L. Yakovlev, G.M. Zhidomirov, R.A. van Santen, J. Phys. Chem. B 105 (2001) 12297.
[84] A.L. Yakovlev, G.M. Zhidomirov, R.A. van Santen, Catal. Lett. 75 (2001) 45.
[85] K. Sun, H. Xia, E. Hensen, R. van Santen, J. Catal. 238 (2006) 186.
[86] L. Que, W.B. Tolman, Angew. Chem. Int. Ed. 41 (2002) 1114.
[87] H. Chen, T. Voskoboinikov, W.M.H. Sachtler, J. Catal. 180 (1998) 171.
[88] E. El-Malki, R.A. van Santen, W.M.H. Sachtler, J. Phys. Chem. B 103 (1999) 4611.
[89] E. El-Malki, R.A. van Santen, W.M.H. Sachtler, J. Catal. 196 (2000) 212.
[90] A.V. Kucherov, M. Shelef, J. Catal. 195 (2000) 112.
[91] P. Marturano, L. Drozdova, A. Kogelbauer, R. Prins, J. Catal. 192 (2000) 236.
[92] P. Marturano, L. Drozdova, G.D. Pirngruber, A. Kogelbauer, R. Prins, Phys. Chem. Chem. Phys. 3 (2001) 5585.
[93] A.A. Battiston, J.H. Bitter, F.M.F. de Groot, A.R. Overweg, O. Stephan, J.A. van Bokhoven, P.J. Kooyman, C. van der Spek, G. Vanko, D.C. Koningsberger, J. Catal. 213 (2003) 251.
[94] A.A. Battiston, J.H. Bitter, W.M. Heijboer, F.M.F. de Groot, D.C. Koningsberger, J. Catal. 215 (2003) 279.
[95] A.A. Battiston, J.H. Bitter, D.C. Koningsberger, J. Catal. 218 (2003) 163.
[96] V. Rakić, V. Rac, V. Dondur, A. Auroux, Catal. Today 110 (2005) 272.
[97] F. Kapteijn, G. Marbán, J. Rodriguez-Mirasol, J.A. Moulijn, J. Catal. 167 (1997) 256.